Title

Sequential Targeting in Crosslinking Nanotheranostics for Tackling the Multibarriers of Brain Tumors

Journal

Advanced Materials, 32(14)

ISSN

0935-9648

Authors

Wu, Hao

Lu, Hongwei

Xiao, Wenwu

et al.

Publication Date

2020-04-01

DOI

10.1002/adma.201903759

Peer reviewed

Published in final edited form as:

Adv Mater. 2020 April ; 32(14): e1903759. doi:10.1002/adma.201903759.

Sequential Targeting in Crosslinking Nano-theranostics for Tackling the Multi-barriers of Brain Tumors

Hao Wu,
Department of Biochemistry and Molecular Medicine, University of California Davis Sacramento, California 95817, Unites States

Hongwei Lu,
Department of Biochemistry and Molecular Medicine, University of California Davis Sacramento, California 95817, Unites States

Wenwu Xiao,
Department of Biochemistry and Molecular Medicine, University of California Davis Sacramento, California 95817, Unites States

Jinfan Yang,
Department of Biochemistry and Molecular Medicine, University of California Davis Sacramento, California 95817, Unites States

Hongxu Du,
Department of Biochemistry and Molecular Medicine, University of California Davis Sacramento, California 95817, Unites States

Yingbin Shen,
Department of Biochemistry and Molecular Medicine, University of California Davis Sacramento, California 95817, Unites States

Haijing Qu,
Department of Biochemistry and Molecular Medicine, University of California Davis Sacramento, California 95817, Unites States

Bei Jia,
Department of Biochemistry and Molecular Medicine, University of California Davis Sacramento, California 95817, Unites States

Suman K Manna,
UC Davis RISE Eye-Pod Laboratory, Department of Cell Biology and Human Anatomy, University of California Davis, Davis, California 95616, Unites States

Mythili Ramachandran,
Department of Biochemistry and Molecular Medicine, University of California Davis Sacramento, California 95817, Unites States

lypli@ucdavis.edu.

Supporting Information

Supporting Information is available from the Wiley Online Library or from the author.

Xiangdong Xue,
Department of Biochemistry and Molecular Medicine, University of California Davis Sacramento, California 95817, Unites States

Zhao Ma,
Department of Biochemistry and Molecular Medicine, University of California Davis Sacramento, California 95817, Unites States

Xiaobao Xu,
Department of Biochemistry and Molecular Medicine, University of California Davis Sacramento, California 95817, Unites States

Zhongling Wang,
Department of Biochemistry and Molecular Medicine, University of California Davis Sacramento, California 95817, Unites States

Yixuan He,
Department of Internal Medicine, School of Medicine, University of California Davis Sacramento, California 95817, Unites States

Kit S. Lam,
Department of Biochemistry and Molecular Medicine, University of California Davis Sacramento, California 95817, Unites States

Robert J. Zawadzki,
UC Davis RISE Eye-Pod Laboratory, Department of Cell Biology and Human Anatomy, University of California Davis, Davis, California 95616, Unites States

Yuanpei Li,
Department of Biochemistry and Molecular Medicine, University of California Davis Sacramento, California 95817, Unites States

Tzu-Yin Lin
Department of Internal Medicine, School of Medicine, University of California Davis Sacramento, California 95817, Unites States

Abstract

The efficacy of therapeutics for brain tumors is seriously hampered by multiple drug delivery barriers, including severe destabilizing effects in blood circulation, the blood-brain barrier/blood-brain tumor barrier (BBB/BBTB) and limited tumor uptake. Here we present a **S**equential **T**argeting **I**n **C**rosslin**K**ing (STICK) nano-delivery strategy to circumvent these important physiological barriers to improve drug delivery to brain tumors. STICK nanoparticles (STICK-NPs) could sequentially target BBB/BBTB and brain tumor cells with surface maltobionic acid (MA) and 4-carboxyphenylboronic acid (CBA), respectively, and simultaneously enhance nanoparticle stability with pH-responsive crosslinkages formed by MA and CBA *in situ*. STICK-NPs exhibited prolonged circulation time (17-fold higher area-under-curve) than free agent, allowing increased opportunities to transpass BBB/BBTB via glucose transporter-mediated transcytosis by MA. Tumor acidic environment then triggered the transformation of STICK-NPs into smaller nanoparticles and revealed secondary CBA targeting moiety for deep tumor

penetration and enhanced uptake in tumor cells. STICK-NPs significantly inhibited tumor growth and prolonged the survival time with limited toxicity in mice with aggressive and chemo-resistant diffuse intrinsic pontine glioma. This formulation tackles multiple physiological barriers on-demand with a simple and smart STICK design. Therefore, these features allow STICK-NPs to unleash the potential of brain tumor therapeutics to improve their treatment efficacy.

Graphical Abstract

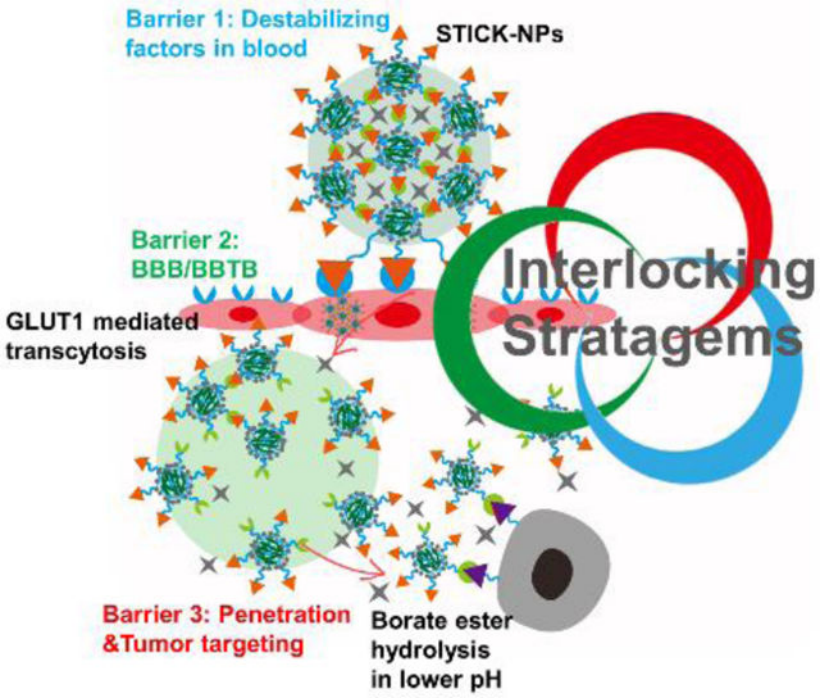

Keywords

sequential targeting; transformable; pH-responsive; blood-brain barrier; diffuse intrinsic pontine glioma

---

Patients with aggressive brain tumors, such as glioblastoma (GBM) or pediatric diffuse intrinsic pontine glioma (DIPG), have a dismal prognosis.[1, 2] Particularly, for DIPG, a devastating and aggressive pediatric brain tumor arising in the ventral pons, radiotherapy is currently the only treatment modality. Children with DIPG have only around 2% five-year survival rate.[2] Many chemotherapeutic drugs such as vincristine (VCR) and novel epigenetic modulating agents, such as inhibitors for Histone deacetylase (HDAC), bromodomains of Bromodomain and Extra-terminal motif (BET), and enhancer of zeste homolog 2 (EZH2) showed promising results in the pre-clinical models.[1, 2] Unfortunately, all the clinical trials on the chemotherapy and epigenetic modulating agents failed to improve the treatment outcome compared to radiation alone.[3] The clinical therapeutic effect of these agents is markedly hampered by the poor drug delivery to brain tumors due to several physiological barriers, including strong destabilizing conditions during the circulation in blood (**Barrier 1**)[4], the blood-brain barrier (BBB)/blood-brain tumor barrier

(BBTB) (**Barrier 2**)[5], poor specificity for targeting tumor cells (**Barrier 3**)[6] and the relatively weak enhanced permeability and retention effect[7] displayed by brain tumors (Figure 1a). There is a clear and urgent need to develop new therapeutic strategies against brain tumors.

BBB was a complex biological barrier, composed of brain endothelial cells, pericytes, astrocytes, tight junctions and basal membrane, to provide a highly regulated barrier essential for maintaining homeostasis and blocking macromolecules, toxin, and infectious agents from the brain.[8-10] The BBTB, similar to the BBB, is a structural-funcitonal barrier located between brain tumor tissue and the microvaculature. With brain tumor progression and aberrant angiogenesis, the BBB gradually becomes impaired and “coverts” into the BBTB.[10, 11] The BBB/BBTB is the main obstacle to drug delivery and limits the efficacy of the brain tumor treatment.[12, 13] A variety of nanocarriers have been reported attempting to circumvent these biological barriers by actively targeting the receptors or transporters on the BBB/BBTB (e.g. glucose transporter 1 (GLUT1)[12, 13], transferrin receptors[14], low-density lipoprotein receptor [15], choline transporter[16], and amino acids transporters[17])) and tumor cell/tissue (e.g. sialic acid[18], integrin family[19], tropomyosin receptor kinase (TRK) family proteins[20], epidermal growth factor receptor (EGFR)[21], and folate receptor[22]), respectively. The BBB/BBTB is a highly regulated barrier that controls the traversal of blood-borne substances into the parenchyma of the central nervous system (CNS) and prevents toxic agents, including chemotherapeutic drugs from entering.[12, 14] Several nutrients including glucose are essential for the brain. The transport of glucose into the CNS is facilitated by GLUT1, which is specifically localized on the BBB/BBTB.[12, 14, 17] Several studies have established that GLUT1 as a validated target for transporter-mediated transcytosis of nanoparticles.[12] It is also known that many types of tumor cells (including those of brain tumors) show an increased sialic acid expression on membrane glycoproteins.[23] The hypersialation of a cell membrane during malignant transformation not only contributes to tumor growth and metastasis but also strongly associates with poor prognosis in cancer patients.[24] Thus, targeting tumor cells by their aberrant sialylation has been an attractive strategy for cancer treatment.[24] GLUT1 and sialic acid, had been separately targeted with different nano-carriers, but had never been dually/sequentially targeted with one particle design.

To tackle the challenge in brain tumor delivery, multifunctional nanoparticles must be designed with consideration of the whole-process in drug deli very to brain tumors as well as the dynamic requirements for each delivery stage. Several dual targeting strategies were developed attempting to address the multiple barriers in brain tumor delivery. For example, a dual-targeting peptide angiopep-2 was decorated on the nanoparticles to target both BBB and GBM cells, and this dual-targeting nanocarrier was demostrated to exhibit superior anti-intracranial GBM effects.[25] He *et al* introduced polysorbate 80 (PS 80) to polymer-bound Trastuzumab (anti-Her2 Antibody) to target both BBB and Her2+ breast cancer brain metastasis.[26] In this system, the first step involved in the PS 80-mediated recruiment of circulating apolipoprotein resulting in transcytosis, and the second step was to target Her2 on breast cancer cells with Trastuzumab after nanoparticle dissociation.[27] While conceptually attractive, these conventional dual targeting design are usually achieved by

simply decorating one or two different targeting moieties on the nanoparticle surface. These moieties ONLY serve for targeting purpose without adding various favorable physical features to the nanoparticle platform to sophisticatedly address the complicated problems in brain tumor delivery.

Herein, we utilized the “Interlocking Stratagems” from *Sun Tzu On The Art of War* and developed a simple-yet-effective Sequential Targeting In CrosslinKing (STICK) nano-delivery approach to improve drug delivery to brain tumors. We strategically selected one unique pair of targeting molecules, maltobionic acid (MA, a glucose derivative) and 4-carboxyphenylboronic acid (CBA) , as our dual targeting moieties for BBB and brain tumor via GLUT1 and sialic acid, respecitvley, to build interlocking STICK nanoparticles (STICK NPs). Beyond targeting functions, this pair of targeting moieties could form pH-sensitive boronate ester bonds to stabilize the nanocarriers with intermicellar crosslinks, thereby benefiting NP stability in blood circulation (**Barrier 1**). Excess MA (a glucose derivative) on the nanoparticle surface can be recognized by GLUT1 and then trigger the GLUT1-mediated BBB/BBTB transcytosis[28] (**Barrier 2**). Upon exposure to the acidic extracellular pH in solid tumors, the intrinsic MA-CBA boronate ester crosslinkages are cleaved,[29] resulting in the transformation of STICK NPs into small secondary nanoparticles with newly unshielded surface CBA (a synthetic mimic of lectin) which allows deeper tumor penetration and recognition of tumor surface sialic acid, respectively[30](Figure 1a) (**Barrier 3**). In this study, we provided a step-by-step proof for the dynamic properties specifically designed to overcome each barrier with STICK approach, including their sequential targeting abilities, pharmacokinetics, and pH-dependent drug release/transformation features. Lastly, we demonstrated their superior anti-cancer targeting abilities using the dual-modality imaging and anti-cancer efficacies in two different aggressive orthotopic brain tumor models.

The principle of STICK approach is to select two different targeting moieties which could also form stimuli-responsive crosslinkages. Considering the barrier 2 and 3 in brain tumor delivery, we choose MA, glucose derivative, for GLUT1-mediated transcytosis through the BBB/BBTB endothelial cells, and CBA which is a type of boronic acid that can target highly expressed sialic acid on brain tumor cells.[18] We built the first STICK-NPs on our previously reported well-characterized micelle platform (nano-micelle (NM) formed by PEG-CA_8).[31] A pair of the telodendrimers, MA_4-PEG-CA_8 and CBA_4- PEG-CA_8, (Figure 1a; Figure S1a, Supporting Information) were synthesized, and the molecular weight, polydispersity index (PdI) and chemical structure of two telodendrimers were characterized by matrix-assisted laser desorption/ ionization time of flight mass spectrometry (MALDI-TOF MS), gel permeation chromatography (GPC) (Figure S1b, Supporting Information) and ^{1}H nuclear magnetic resonance spectroscopy (^{1}H-NMR) (Figure S1c,d, Supporting Information), respectively. Similar to PEG-CA_8, both MA_4-PEG-CA_8 and CBA_4-PEG-CA_8 telodendrimers could individually form well-defined small (Z-average size: 24.5 ± 0.7 nm, 26.2 ± 0.3 nm, 23.0 ± 0.3 nm; PdI: 0.218 ± 0.015, 0.287 ± 0.017, 0.175 ± 0.031, respectively) spherical nanoparticles with a narrow size distribution (Figure 1b; Figure S2a,b, Figure S3a,b, Fiugre S4 and Figure S5, Supporting Information). In order to realize sequential targeting, for the first stage brain endothelial cells, a higher ratio of MA telodendrimer is required to remain free MA targeting moiety on the nanoparticle surface

after forming boronate ester bonds with a lower ratio of CBA telodendrimer (Figure 1c). Thus, different ratios (1:1, 5:1, and 9:1) of MA_4-PEG-CA_8 and CBA_4-PEG-CA_8 were mixed to form STICK-NPs. The intensity-weighted distribution, Z-average size, PdI, and brain endothelial cell targeting ability were assessed using dynamic light scatter (DLS) and fluorescence image, respectively (Figure S2a-c, Supporting Information). We discovered that with the increase of the MA_4-PEG-CA_8 ratio, the size of resulting nanoparticles and endothelial cell targeting ability increased, while the PdI had a different behavior, that increased firstly, reached a maximum (5:1) and then decreased at the ratio of (9:1). Considering all the factors mentioned above, the 9:1 ratio of MA_4-PEG-CA_8 and CBA_4-PEG-CA_8 were determined as the optimal ratio as this formulation gave the most uniform nanoparticle (lowest PdI) among all ratios. Other ratios appeared to form both large and small nanoparticles indicating possible increased intramicelle crosslinkages (formed inside small micelles). Unlike the small micelles (Figure 1b, Figure S4, Supporting Information) formed based on one species of telodendrimers, STICK-NPs (Figure 1b,d; Figure S4, Supporting Information) were relatively large spherical in shape, and contained numerous smaller secondary micelles with a comparable size to non-crosslinked micelles (Figure 1b,d; Figure S5, supporting information). With the decrease of the pH (7.4 to 6.5), boronate ester bonds degraded and STICK-NPs (Z-average size: 137.8 ± 14.2 nm; PdI: 0.230 ± 0.046; TEM size: 92 ± 21 nm) were dissociated into numerous smaller secondary micelles (Z-average size: 25.2 ± 0.2 nm; PdI: 0.207 ± 0.005; TEM size: 14 ± 3 nm, Figure 1d; Figure S4, supporting information). The cut-off pH value for pH-dependent transformation of STICK-NPs is around 6.8 (Figure 1e; Figure S6, Supporting Information), and the transformation took place as early as 5 min and completed at around 1 hour upon exposure to pH 6.5 environment (Figure 1f; Figure S7, Supporting Information).

Another particular feature of STICK-NPs is their capability to encapsulate both hydrophobic and hydrophilic payloads, which offers a significant advantage over conventional micelles that generally only load hydrophobic drugs. STICK-NPs were self-assembled selectively in low-polarity solvents into core-inversible micelles driven by hydrophilic interactions and formed plenty of hydrophilic spaces as reported in another study.[32] The formation of intermicellar crosslinkages preserves the hydrophilic spaces in the subsequent assembly procedures in aqueous solution together with the newly formed hydrophobic cores. This allows the trapping of hydrophilic agents between secondary micelles and hydrophobic agents in the hydrophobic cholic acid core, like other control micelles (Figure 1a). We already demonstrated both hydrophilic agents (e.g. indocyanine green (ICG), gadopentetic acid (Gd-DTPA), doxorubicin hydrochloride (DOX·HCl)) and hydrophobic agents (e.g. Cyanine7.5 (Cy7.5), 1,1’-Dioctadecyl-3,3,3’,3’-tetramethylindodicarbocyanine 4-chlorobenzenesulfonate (DiD), VCR and paclitaxel (PTX)) could be encapsulated into STICK-NPs with high loading efficiency (Table S1, Supporting Information). Gd-DTPA and Cy7.5 could be co-loaded together into STICK-NPs with a Z-average size of 140.2 ± 11.8 nm for a variety of theranostic applications as shown in the subsequent sections.

To validate our hypothesis, we formulated STICK-NPs in diverse solvents with various polarities (Figure 1g). In a nonpolar solvent, the size of the inversible micelles was maintained at over 116 nm even with the solvent evaporation and re-hydration in phosphate-buffered saline (PBS). Even strong detergents, such as sodium-dodecyl sulfate (SDS), failed

to break down the micelles, as MA_4-PEG-CA_8 and CBA_4-PEG-CA_8 were able to form stable intermicellar crosslinkages in the presence of a nonpolar solvent. In contrast, in polar solvents, MA_4-PEG-CA_8 and CBA_4-PEG-CA_8 were not able to form core-inversible micelles and the final nanoparticles showed a smaller size as compared to other control micelles. Such smaller micelles could be easily destroyed in the presence of SDS (Figure 1g), which was likely due to the lack of formation of enough boronate cross-linkages to stabilize the nanoparticles.

The distinctive drug loading in different compartments of STICK-NPs led to different drug release profiles of the hydrophilic and hydrophobic payloads in response to pH changes. Hydrophilic Gd-DTPA and hydrophobic Cy7.5 dye were used as model drugs for co-loading into STICK-NPs, and a drug release study was performed in pH 7.4 medium initially and then in pH 6.5 medium after 4 hours (Figure 2a,b). This experiment was purposely designed to model the two-stage *in vivo* drug release (pH 7.4 in blood and pH 6.5 in tumor microenvironment), as described previously.[13] Hydrophilic Gd-DTPA could not be loaded into NMs efficiently, and thus NM+ free Gd-DTPA was used in this study. Figure 2a showed that free Gd-DTPA was released immediately, while Gd-DTPA was released from STICK-NPs at a much lower rate but could be accelerated upon changing to pH 6.5 solution. This was because hydrophilic Gd-DTPA was trapped between micelles and could gradually diffuse but only rapidly release upon pH-dependent cleavage of intermicellar crosslinkages. The release rate of hydrophobic Cy7.5 loaded in the hydrophobic interior of secondary micelles of STICK-NPs was dramatically slower than that of Gd-DTPA at pH7.4, which is likely due to the hydrophobic property of Cy7.5 (Figure 2b). At acidic pH, the release of Cy7.5 from STICK-NPs was slightly enhanced, probably due to the mild crosslinkage formed within the secondary micelles. In contrast, Cy7.5 loaded non-crosslinked non-targeting micelles (NM@Cy) showed faster drug release under pH7.4 and had minimal response to pH changes as there were no pH-responsive crosslinkages (Figure 2b). These results demonstrated that STICK-NP can rapidly release hydrophilic drugs in a lower-pH responsive manner and deliver hydrophobic drugs into tumors through a secondary micelle release mechanism. Taking advantage of the co-loaded Cy7.5 and Gd-DTPA, STICK-NPs could potentially be applied for dual-modal imaging (magnetic resonance imaging (MRI) and near-infrared fluorescence (NIRF) imaging) (Figure 2c; Figure S3c-e, Supporting Information). Upon exposure to a lower pH environment, STICK-NP@Cy@Gd transformed and released hydrophilic Gd-DTPA, resulting in a recovered T_1 signal comparable to that of free Gd-DTPA. The r_1 of STICK-NP@Cy@Gd increased from 1.061 $mM^{-1}*s^{-1}$ to 4.447 $mM^{-1}*s^{-1}$ when the pH was changed from 7.4 to 6.5 (Figure S3e, Supporting Information).

The first biological barrier for brain tumor nanoparticle delivery is the strong destabilizing effects in blood circulation that includes: extreme dilution, an ionic environment, and interaction with blood proteins and lipoproteins (e.g. HDL, LDL), resulting in nanoparticle dissociation and premature drug release.[33] Stabilized by inter-micellar crosslinkages, STICK-NP@Cy@Gd retained their size in PBS and even in the presence of 50 mM SDS and 10% FBS/PBS over a period of 35 days (Figure 2d). Since STICK was dependent on the formation of the boronate ester bond between CBA and MA (glucose derivative with two cis-diols), there was a concern for the possible competition from the serum glucose resulting in the degradation of crosslinkages. Therefore, we performed additional experiments and

demonstrated that crosslinkage was very stable at the physiological levels of glucose and up to a glucose concentration reaching 100 mmol/L (Figure 2e; Figure S8, Supporting Information). Of note, the level of serum glucose for healthy human is around 3.9-5.5 mmol/L (70-100 mg/dL),[34] and even patients suffering from diabetes are unlikely to reach a glucose level of 50 mmol/L. Additionally, STICK-NP performed exceptionally in a pharmacokinetic study in rats. Compared to conventional NM and free Cy7.5 formulations, STICK-NP@Cy@Gd increased the area under the curve ($AUC_{(0-\infty)}$) by 5.4 times and 17.6 times, respectively (Figure 2f; Table S2, Supporting Information). Besides, STICK-NP@Cy exhibited the highest C_{max} (35.0 ± 3.6 mg/L, or 5 times higher than NM@Cy), and longest $t_{1/2z}$ (34.7 ± 12.1 hours, or 2 times longer than NM@Cy). These results strongly support that STICK-NPs exhibited superior stability during circulation and prevented premature drug release due to inter-micellar crosslinkages. Such improvements that significantly increase systemic circulation time offer a prolonged drug delivery window to brain tumors.

The second barrier encountered by the STICK-NPs is the BBB/BBTB, tight junctions formed by the brain microvessel endothelial cells.[6] Excess ratios of MA (glucose derivative) on STICK-NPs are the first exposed targeting moiety for GLUT1 mediated endothelial cell transcytosis, while CBA is shielded in the STICK (Figure 1a). To validate our hypothesis, we cultured mouse brain endothelial cells (bEnd.3) cells in the top chamber of a Transwell® system and the formation of the tight junctions was confirmed by the transendothelial electrical resistance (TEER) > 200 $\Omega.cm^2$ (Figure 3a).[8, 35] The evaluation of the total fluorescence intensities in the bEnd.3 cells (during transcytosis) (Figure 3b; Figure S10, Supporting Information) and the medium in the lower chamber (post-transcytosis) (Figure 3c) were performed at different time points after loading nanoparticles on the top chamber. Figure 3b demonstrated that STICK-NP@Cy and MA-NP@Cy (also targeting GLUT1 via MA) had the highest intracellular signals among all groups. Consistent with this finding, STICK-NP@Cy and MA-NP@Cy groups had the highest tight-junction transversed amounts into the lower chambers (Figure 3c). When GLUT1 was blocked by the GLUT1 inhibitor (WZB-117) (Figure S9a,b, Supporting Information), the transverse of STICK-NP@Cy was diminished. The most intriguing finding was that the size of the STICK-NP@Cy remained similar before transcytosis and after transcytosis through bEnd.3 cells when comparing the size of STICK-NP@Cy in the upper and lower chambers (Figure 3d). When we assessed the subcellular distribution of STICK-NP@DiD in bEnd.3 cells, we discovered that STICK-NP@DiD did not co-localize with lysosome with a low Pearson's coefficient index of 0.057.[36] Presumably, the low lysosomal pH (5.5) should have destroyed the crosslinkages and initiated the release of secondary smaller micelles if a lysosomal-dependent pathway occurred. Those collective evidence supported our notion that STICK-NP transpass BBB probably via a transytosis pathway and further detailed mechanism studies are undergoing.

As orthotopic brain tumor model may not have intact BBB due to mechanical disruption, we decided to validate the ability of the STICK-NPs for delivery of the poor brain permeable chemotherapeutic drug (VCR)[3] *in vitro* and in normal Balb/c mice. Similarly, STICK-NP@VCR could transpass brain endothelial cells and deliver significantly higher VCR to the lower chamber, compared to free and NM@VCR in the BBB transwell modeling system (Figure S9c, Supporting Information). In the Balb/c model, at 6 hours post-injection, whole

brains were harvested and tissue drug concentrations were measured by LC/MS. We demonstrated around double amounts of VCR retained in the normal brain parenchyma after STICK-NP@VCR, compared to free VCR, or other non- or single targeting formulations (Figure 3f). Collectively, these results confirmed that STICK-NPs could efficiently transverse the BBB/BBTB via GLUT1 mediated transcytosis.

Lastly, after passing through the BBB, STICK-NPs then enter the acidic tumor microenvironment (Barrier 3). In response to the lower extracellular pH, STICK was broken down resulting in the release of secondary small micelles (Figure 3d,g). CBA was originally shielded as part of STICK and now to be exposed after cleavage of crosslinking as the secondary tumor targeting moiety for brain tumors (Figure 1a and Figure 3g). Next, we investigated the brain tumor cell targeting and cellular uptake abilities of secondary STICK-NPs using fluorescence imaging. Human U87-MG (GBM) cells were treated with STICK-NP@Cy and other control formulations under both pH 7.4 and pH 6.5 for 4 hours (Figure 3h, i). Results demonstrated that the overall cellular uptake was relatively lower at pH 7.4 in all groups, including STICK-NPs with shielded CBA. In contrast, pretreatment with pH 6.5 exposed CBA which significantly enhanced brain tumor cell uptake of STICK-NP@Cy. Conversely, there was no significant enhancement in free Cy7.5, MA-NP@Cy, CBA-NP@Cy, and NM@Cy groups even with pre-treatment at pH 6.5. To further explore the potential role of sialic acid expression in the nanoparticle uptake, cells were treated with 3-Azidothymidine (AZT) to increase surface sialic acid expression.[37] Such treatment further facilitated tumor cell uptake of STICK-NPs (pH 6.5) (Figure 3h-j). Furthermore, the CBA mediated cellular uptake of STICK-NPs (pH 6.5) could be radically blocked by excess free CBA (Figure 3h-j). These results proved that STICK-NPs could be effectively uptaken by brain tumor cells after transformation, which is likely due to the newly revealed CBA to enhance the sialic acid-mediated transcytosis. It was worth considering that under pH 6.5, CBA has a much higher affinity toward sialic acid than glucose (as MA), and thus would preferably bind to sialic acid on tumor cells.[18]

To model the combination of barrier 2 (BBB/BBTB) and barrier 3 (brain tumor uptake) in delivery to brain tumors, we cultured bEnd.3 cells in the upper chamber of Transwell and U87-MG brain tumor cells in the lower chamber (Figure 3k). STICK-NP@Cy and other control NPs were loaded in the upper chamber for 1 hour and the pH of the medium in the lower chamber was adjusted to 7.4 or 6.5 for an additional 1 hour allowing U87-MG tumor cell uptake. As expected, Figure 3l, m shows that STICK-NP@Cy (pH 6.5) group achieved the highest uptake in U87-MG cell compared to STICK-NP@Cy (pH7.4), MA-NP@Cy, CBA-NP@Cy, and NM@Cy (pH7.4 and 6.5) groups or free dye in the lower chamber. GLUT1 inhibition also impeded the final U87-MG cell uptake potentially due to decreased transcytosis (Figure 3b,c). Those results altogether provided a step-by-step validation of the mechanisms for the significantly enhanced drug delivery of STICK-NPs including BBB/BBTB transcytosis, transformation, and tumor cellular uptake. Importantly, single targeting nanoparticles either with CBA or MA may slightly improve the delivery to brain tumors but the efficiency was still sub-optimal in comparison.

After transcytosis and transformation, STICK-NPs released numerous secondary micelles, which is more suitable for deep tissue penetration in tumors (Figure 1b,d; Figure S5,

Supporting Information). The three-dimensional multicellular spheroid system most resembles *in vivo* conditions and forms a compact extracellular matrix environment allowing for testing of drug penetration *in vitro*.[24] To assess the size-dependent tissue penetration effects, we incubated the U87-MG neurosphere (~400 μm) with STICK-NP@DiD and other control formulations under pH 7.4 or 6.5. After 24 hours, confocal fluorescence imaging of U87-MG spheroid showed that non-transformed STICK-NP@DiD (pH 7.4) group had poor penetration and lower penetration depth (30.1 μm ± 5.9 μm) (Figure 4a; Figure S11, Supporting Information) due to its relatively large size (Figure 1b; Figure S5, Supporting Information). Upon pH-dependent transformation, STICK-NP@DiD (pH 6.5) possessed significantly superior penetration ability compared to STICK-NP@DiD (pH 7.4) and reached a similar depth compared to other nanoformulations with a small size (Figure 4a and Figure 1b; Figure S5 and Figure S11, Supporting Information). Similar pH dependent transformation/penetration effects were further confirmed in the DIPG patient-derived xenograft (PDX) neurosphere (~300 μm in diameter) (Figure 4b). The pH-responsive feature actually equips STICK-NP with tumor selectivity. Accordingly, we employed an orthotopic DIPG model to evaluate the degree of the tissue penetration of STICK-NPs at both normal brain and acidic tumor sites. Figure 4c, d showed that at 24 hours, STICK-NP@DiD were able to penetrate into DIPG tumor tissue around 30 μm far from the blood vessels. In contrast, in the normal brain parenchyma (reported dog brain parenchyma pH was 7.13[38]), STICK-NP@DiD only penetrated around 5 μm beyond the blood vessel. Meanwhile, NM@DiD control had minimal normal brain penetration ability (Figure 4c). Along with the *in vitro* studies, we concluded that STICK-NP could be selectively responsive to the acidic environment to release secondary nanoparticles with newly revealed CBA targeting moiety allowing better tumor tissue penetration and tumor cell uptake. With the pH selectivity, STICK-NP would have limited normal tissue penetration and less concern for neurotoxicity.

We next utilized an orthotopic PDX GBM model to evaluate the biodistribution of STICK-NPs@Cy@Gd using the dual-modality imaging: NIRF imaging (Cy7.5) and MRI (Gd-DTPA) (Figure 5a). At 10 min post-injection, all groups had increased overall brain MRI T_1 weighted signals (Figure 5a). At 24 and 48 hours post-injection, STICK-NP@Cy@Gd groups had both significantly higher T_1-weighted MRI signal intensity (Figure 5a,b) and Cy7.5 fluorescence intensity (Figure 5a,c,d) at the tumor sites, compared to free Cy7.5+Gd, NM@Cy+Gd, CBA-NP@Cy+Gd, and MA-NP@Cy+Gd groups. It is important to note that unlike in STICK-NPs, hydrophilic Gd-DTPA could not be loaded in the NM, CBA-NPs, and MA-NPs and thus were injected as free Gd-DTPA in those groups along with Cy7.5 loaded nanoparticles as control groups. The NIRF or T_1-weight MRI signals of STICK-NP@Cy@Gd were maintained in the tumors for the longest time and only returned to baseline at 72 hours post-injection (Figure S12a, Supporting Information). Although we only used 1/3 of the clinical dose of Gd-DTPA,[39] it appeared that this particular PDX model exhibited poor permeability, evidenced by the minimal T_1 signals of Gd-DTPA presented at the tumors sites at 10 min (Figure 5a). Nevertheless, STICK-NPs could still efficiently target, penetrate, and retain in the PDX GBM model.

To further dissect the target delivery efficiency and selectivity into the brain tumor, another set of mice were sacrificed at 24 hours post nanoparticle administration and major organs/brain with brain tumors were harvested for *ex vivo* NIRF imaging. Biodistribution was

assessed based on the Cy7.5 signals in the brain and other major organs. As shown in Figure 5a,d, Figure S12b,c, Supporting Information, STICK-NPs could specifically deliver a higher concentration of Cy7.5 to the orthotopic PDX GBM tumors compared to other major organs, excepting the kidney, which could potentially be the clearance route for Cy7.5 dye. The STICK-NPs treated group had a significantly higher accumulation of the Cy7.5 signals at the brain tumor sites, comparing to free Cy7.5+Gd and NM@Cy+Gd. NIRF imaging of cryosections from the orthotopic brain tumors in the STICK-NPs group exhibited a strong correlation between tumor cells (green) and Cy7.5 (red) (Figure 5e; Figure S12d, Supporting Information) with a calculated Pearson's coefficient index of up to 0.637. Meanwhile, the normal brain had minimal uptake suggesting the excellent tumor selectivity of STICK-NPs (Figure 5c,e). The semi-quantitative imaging analysis demonstrated that orthotopic GBM PDX tumor had around 1.5 times and 4 times higher signals than adjacent normal brain tissues on MRI and NIRF imaging, respectively (Figure 5b,d).

The targeted delivery of STICK-NPs was further investigated in an orthotopic DIPG PDX model. We firstly used Gd-enhanced T_1-weighted MRI to locate DIPG. After the clearance of the Gd signal, the mice were re-injected with DiD+Gd, NM@DiD+ Gd, and STICK-NPs@Gd@DiD and re-imaged at 16 hours post-injection (Figure 5f). As shown in Figure 5f, STICK-NPs@Gd@DiD selectively and efficiently concentrated at the tumor sites as shown in both imaging modalities. The imaging studies served as strong support that STICK-NP@Cy@Gd could specifically deliver payloads to the tumor sites allowing accurate imaging-guided drug delivery and potential utilization for delineation of tumor margins during surgery. In contrast, single target formulations, MA-NPs, and CBA-NPs which previously showed their targeting effects *in vitro*, were not able to deliver sufficient payload to orthotopic brain tumors *in vivo*.

VCR is a mainstay of treatment for a variety of pediatric and adult cancers including brain tumor due to its well-defined mechanism of action and demonstrated anticancer activity. However, its effectiveness in brain tumors is realtively limited particularly due to dose-limiting neurotoxicity and its inability to penetrate into brain tumor resulting in limited anti-cancer efficacy.[40] Hence, in this study, we employed STICK-NPs to deliver VCR and evaluated their anti-cancer effects in a very aggressive and infiltrating orthotopic DIPG brain tumor model. Pediatric DIPG cells were injected into the pons of the SCID mouse brain to establish orthotopic model. After confirming the establishment of the DIPG brain tumors in mice using Gd-enhanced T_1 weighted MRI (Figure 6a), mice were randomly assigned into 9 groups: PBS, 1.5 mg/kg free VCR, NM@VCR, MA-NP@VCR, CBA-NP@VCR, STICK-NP@VCR and Marqibo® (liposomal VCR), and two high dose groups, free VCR2 and STICK-NP@VCR2 (VCR 2 mg/mL) (n = 6). Since this is a very aggressive DIPG model, free VCR (1.5 and 2 mg/kg), NM@VCR, MA-NP@VCR, CBA-NP@VCR, and Marqibo®, all had minimal inhibition effects on tumor growth and failed to extend the survival of the animals compared to PBS control (Figure 6a-d). Very encouragingly, STICK-NP@VCR exhibited promising effects in hindering tumor growth (Figure 6a-c; Figure S13, Supporting Information) and almost doubled the survival times (21.3 days) compared to Marqibo®, CBA-NP@VCR and MA-NP@VCR (survival time 12.5 days, 12 days and 12 days, respectively) (Figure 6d). Even at the higher dose (2mg/kg), VCR had no benefit in the survival time of DIPG bearing mice (Figure 6a-c). In contrast, STICK-NP@VCR at the

equivalent dose level could further prolong the overall survival time, and 2 out of 6 mice in this group survived over 50 days. To achieve the best results, we continuously treated the remaining animals with 2 mg/kg of STICK-NP@VCR every 6 days. The orthotopic DIPG tumors in these mice were completely eradicated. During the treatment period, there were no significant changes in body weight, until the development of the neurological syndrome due to increased tumor burden and invasion (Figure 6e; Figure S14, Supporting Information). Additionally, we performed a similar efficacy study in a more vascularized GBM orthotopic model in nude mice (Figure S15, Supporting Information). STICK-NP@VCR consistently outperformed other formulations with only a single dose of 2 mg/kg VCR. STICK@VCR significantly impeded tumor progression based on both MRI and histopathology (Figure S15a,d, Supporting Information) and prolonged the median survival times (34 days), compared to other formulations (all less than 17 days). Major organs were also harvested on day 12 post-treatment, and no major pathological changes were identified in all groups (Figure S15f, Supporting Information). Altogether, these efficacy studies strongly supported our hypothesis that STICK-NPs could efficiently deliver a high dose of the chemotherapeutic drug to the tumor site and eradicate brain tumors with limited toxicity. The disappointing anti-cancer results by either CBA or MA single targeting nanoparticles restates the need to consider the complexity and dynamic circumstances during brain tumor delivery.

In summary, our innovative STICK strategy provides a simple but smart solution in tackling multiple barriers in drug delivery to brain tumors. STICK was designed based on a unique pair of two targeting moieties which could also form a stimuli-responsive bond, such as glucose derivatives and boronic acid families which could form pH-responsive boronate crosslinkages. In the current STICK approach, the targeting moieties (CBA or MA) serve much more than targeting purpose. They are integrated into the nanoparticle architecture and significantly contribute the desirable characteristics (e.g. stablity, stimuli-responsiveness, transformability and versatile drug loading capability) and overall delivery performance of these nanoparticles. Such a unique STICK design clearly distinguishes itself from previously published dual targeting systems. We introduced STICK strategy into our well-characterized micelle formulation[31] and showed that STICK-NPs could survive in the bloodstream and sequentially STICK into the BBB/BBTB and brain tumor cells, respectively. We demonstrated that STICK-NPs could overcome the destabilizing environment in blood with the inter-micellar crosslinkages formed by MA (exposed) and CBA (shielded) and showed significantly prolonged circulation time allowing a wider brain tumor targeting window (Figure 1). During circulation, surface excess MA on the nanoparticle could facilitate GLUT1-mediated transcytosis through BBB/BBTB to “actively” target brain tumors (Figure 3). Subsequently, the STICK was cleaved after encountering the intrinsic acidic pH at the tumor sites, triggering the transformation into secondary smaller nanoparticles for deep tumor tissue penetration (Figure 4), and revealing the secondary targeting moiety, CBA against the sialic acid overexpressed in tumor cells for enhanced cellular uptake (Figure 5). The pH-dependent selectivity further endowed their biosafety features. In the orthotopic GBM and DIPG mouse models, STICK-NPs effectively delivered both hydrophobic and hydrophilic image agents to tumor sites for the dual-modality imaging. Most excitingly, STICK-NP@VCR exhibited superior brain tumor inhibition effect and dramatically

prolonged survival time even in the most aggressive and VCR-resistant DIPG model in comparison to the single targeting formulations (Figure 6). These promising results highlighted the unique feature of STICK at overcoming different complicated barriers and the importance of considering all the obstacles during nanoparticle design for successful brain tumor delivery. Given the versatile drug loading capability, STICK-NP could provide the immediate second hope to deliver the most advanced epigenetic modulating agents, such as HDAC and EZH2 inhibitors,[1, 41] which efficacies were greatly hindered by the BBB/BBTB resulting in failed clinical trials. Given the extremely versatile STICK platform and its ability to co-load both hydrophobic and hydrophilic drugs/dyes, STICK NP could also be potentially utilized for the combination of chemotherapy (such as VCR and Temozolomide), molecular targeting agents (such as CDK4/6 inhibitor and mTOR inhibitor), and/or epigenetic modulators against brain tumors.[42] Our research not only provides noteworthy opportunities to apply STICK approach to many other nanoformulation designs against dynamic and entanglement biological barriers but also have animpact in advancing the drug development/delivery for aggressive brain tumors.

Supplementary Material

Refer to Web version on PubMed Central for supplementary material.

Acknowledgements

We thank the financial support from NIH/NCI (R01CA199668, 1R01CA232845, K12CA138464), NIH/NICHD (R01HD086195, R43 HD097970-01) and UC Davis Comprehensive Cancer Center Support Grant (CCSG) awarded by the National Cancer Institute (NCI P30CA093373). The UC Davis EyePod development and studies were supported by NIH/NCI U01 CA198880, NIH/NEI R01 EY01256, R01 EY026556 and UC Davis Small Animal Ocular Imaging NEI Core 5P30 EY012576.

References

[1]. Mohammad F, Weissmann S, Leblanc B, Pandey DP, Hojfeldt JW, Comet I, Zheng CQ, Johansen JV, Rapin N, Porse BT, Tvardovskiy A, Jensen ON, Olaciregui NG, Lavarino C, Sunol M, de Torres C, Mora J, Carcaboso AM, Helin K, Nat. Med 2017, 23, 483. [PubMed: 28263309]

[2]. Buczkowicz P, Hoeman C, Rakopoulos P, Pajovic S, Letourneau L, Dzamba M, Morrison A, Lewis P, Bouffet E, Bartels U, Zuccaro J, Agnihotri S, Rya S, Barszczyk M, Chornenkyy Y, Bourgey M, Bourque G, Montpetit A, Cordero F, Castelo-Branco P, Mangere J, Tabori U, Ching K, Huang A, Taylor KR, Mackay A, Bendell AE, Nazarian J, Fangusaro JR, Karajannis MA, Zagzag D, Foreman NK, Donson A, Hegert JV, Smith A, Chan J, Lafay-Cousin L, Dunn S, Hukin J, Dunham C, Scheinemann K, Michaud J, Zelcer S, Ramsay D, Cain J, Brennan C, Souweidane MM, Jones C, Allis CD, Brudno M, Becher O, Hawkins C, Nat. Genet 2014, 46, 451. [PubMed: 24705254]

[3]. Hashizume R, Neurol. Med. Chir 2017, 57, 331;La Madrid AM, Hashizume R, Kieran MW, Front. Oncol 2015, 5.

[4]. Zhu QW, Chen XJ, Xu X, Zhang Y, Zhang C, Mo R, Adv. Funct. Mater 2018, 28.

[5]. Wu D, Qin M, Xu D, Wang L, Liu C, Ren J, Zhou G, Chen C, Yang F, Li Y, Adv. Mater 2019, 1807557;He QG, Liu J, Liang J, Liu XP, Li W, Liu Z, Ding ZY, Tuo D, Cells 2018, 7;Chen WS, Ouyang J, Yi XY, Xu Y, Niu CC, Zhang WY, Wang LQ, Sheng JP, Deng L, Liu YN, Guo SJ, Adv. Mater 2018, 30.

[6]. Banks WA, Nat. Rev. Drug Discov 2016, 15, 275; [PubMed: 26794270] Qian TC, Maguire SE, Canfield SG, Bao XP, Olson WR, Shusta EV, Palecek SP, Sci. Adv 2017, 3.

[7]. Meyers JD, Doane T, Burda C, Basilion JP, Nanomedicine 2013, 8, 123; [PubMed: 23256496] Wu L, Li X, Janagam DR, Lowe TL, Pharm. Res 2014, 31, 531; [PubMed: 23996470] Liu Y, Lu W,

Expert Opin. Drug Del 2012, 9, 671;Ruan SB, He Q, Gao HL, Nanoscale 2015, 7, 9487. [PubMed: 25909483]

[8]. Lu Z, Li Y, Shi Y, Li Y, Xiao Z, Zhang X, Adv. Funct. Mater 2017, 27, 1703967.

[9]. Dong X, Theranostics 2018, 8, 1481. [PubMed: 29556336]

[10]. Hersh DS, Wadajkar AS, Roberts N, Perez JG, Connolly NP, Frenkel V, Winkles JA, Woodworth GF, Kim AJ, Curr Pharm Des 2016, 22, 1177. [PubMed: 26685681]

[11]. S Hersh D, S Wadajkar A, B Roberts N, G Perez J, P Connolly N, Frenkel V, A Winkles J, F Woodworth G, J Kim A, Curr. Pharm. Design 2016, 22, 1177;Dong X, Theranostics 2018, 8, 1481; [PubMed: 29556336] Garg T, Bhandari S, Rath G, Goyal AK, J. Drug Target.ing 2015, 23, 865.

[12]. Wei X, Chen X, Ying M, Lu W, Acta Pharm. Sin. B 2014, 4, 193; [PubMed: 26579383] Stalmans S, Bracke N, Wynendaele E, Gevaert B, Peremans K, Burvenich C, Polis I, De Spiegeleer B, PloS one 2015, 10, e0139652; [PubMed: 26465925] Paterson J, Webster CI, Drug. Discov. Today 2016, 20, 49.

[13]. Ruan SB, Qin L, Xiao W, Hu C, Zhou Y, Wang RR, Sun X, Yu WQ, He Q, Gao HL, Adv. Funct. Mater 2018, 28.

[14]. Lam FC, Morton SW, Wyckoff J, Han TLV, Hwang MK, Maffa A, Balkanska-Sinclair E, Yaffe MB, Floyd SR, Hammond PT, Nat. Commun 2018, 9.

[15]. Serna N, Cespedes MV, Saccardo P, Xu ZK, Unzueta U, Alamo P, Pesarrodona M, Sanchez-Chardi A, Roldan M, Mangues R, Vazquez E, Villaverde A, Ferrer-Miralles N, Nanomed.-Nanotechnol 2016, 12, 1241.

[16]. Li JF, Guo YB, Kuang YY, An S, Ma HJ, Jiang C, Biomaterials 2013, 34, 9142. [PubMed: 23993342]

[17]. Neuwelt EA, Bauer B, Fahlke C, Fricker G, Iadecola C, Janigro D, Leybaert L, Molnar Z, O'Donnell ME, Povlishock JT, Saunders NR, Sharp F, Stanimirovic D, Watts RJ, Drewes LR, Nat. Rev. Neurosci 2011, 12, 169. [PubMed: 21331083]

[18]. Wang X, Wei B, Cheng X, Wang J, Tang RP, Eur. J. Pharm. Biopharm 2017, 113, 168. [PubMed: 28089786]

[19]. Friedland JC, Lee MH, Boettiger D, Science 2009, 323, 642. [PubMed: 19179533]

[20]. Khotskaya YB, Holla VR, Farago AF, Shaw KRM, Meric-Bernstam F, Hong DS, Pharmacol. Therapeut 2017, 173, 58.

[21]. Van Grembergen O, Bizet M, de Bony EJ, Calonne E, Putmans P, Brohee S, Olsen C, Guo MZ, Bontempi G, Sotiriou C, Defrance M, Fuks F, Sci. Adv 2016, 2.

[22]. Wu H, Wang HH, Liao H, Lv Y, Song XJ, Ma XJ, Tan MQ, Adv. Healthc. Mater 2016, 5, 311. [PubMed: 26626703]

[23]. Bull C, Stoel MA, den Brok MH, Adema GJ, Cancer Res. 2014, 74, 3199. [PubMed: 24830719]

[24]. Ji M, Li P, Sheng N, Liu L, Pan H, Wang C, Cai L, Ma Y, ACS Appl. Mater. Inter 2016, 8, 9565.

[25]. Qiao C, Yang J, Shen Q, Liu R, Li Y, Shi Y, Chen J, Shen Y, Xiao Z, Weng J, Adv. Mater 2018, 30, 1705054.

[26]. He CS, Li JS, Cai P, Ahmed T, Henderson JT, Foltz WD, Bendayan R, Rauth AM, Wu XY, Adv. Funct. Mater 2018, 28.

[27]. Li Y, He H, Jia X, Lu W-L, Lou J, Wei Y, Biomaterials 2012, 33, 3899; [PubMed: 22364698] Kim JS, Shin DH, Kim J-S, Control J. Release 2018, 269, 245;Chen M, Chen R, Shi Y, Wang JG, Cheng YH, Li Y, Gao XD, Yan Y, Sun JZ, Qin AJ, Kwok RTK, Lam JWY, Tang BZ, Adv. Funct. Mater 2018, 28.

[28]. Deng D, Yan N, Protein Sci. 2016, 25, 546. [PubMed: 26650681]

[29]. Rocha PRF, Medeiros MCR, Kintzel U, Vogt J, Araujo IM, Mestre ALG, Mailander V, Schlett P, Droge M, Schneider L, Biscarini F, de Leeuw DM, Gomes HL, Sci. Adv 2016, 2;Yesilyurt V, Webber MJ, Appel EA, Godwin C, Langer R, Anderson DG, Adv. Mater 2016, 28, 86; [PubMed: 26540021] Karimi M, Ghasemi A, Zangabad PS, Rahighi R, Basri SMM, Mirshekari H, Amiri M, Pishabad ZS, Aslani A, Bozorgomid M, Ghosh D, Beyzavi A, Vaseghi A, Aref AR, Haghani L, Bahrami S, Hamblin MR, Chem. Soc. Rev 2016, 45, 1457; [PubMed: 26776487] Wang Y, Zhou K, Huang G, Hensley C, Huang X, Ma X, Zhao T, Sumer BD, DeBerardinis RJ, Gao J, Nat.

Mater 2014, 13, 204; [PubMed: 24317187] Lang TQ, Liu YR, Zheng Z, Ran W, Zhai YH, Yin Q, Zhang PC, Li YP, Adv. Mater 2019, 31.

[30]. Wang X, Tang H, Wang C, Zhang J, Wu W, Jiang X, Theranostics 2016, 6, 1378. [PubMed: 27375786]

[31]. Li Y, Xiao W, Xiao K, Berti L, Luo J, Tseng HP, Fung G, Lam KS, Angew. Chem. Int. Edit 2012, 51, 2864.

[32]. Huang WZ, Shi CY, Shao Y, Lamb KS, Luo JT, Chem. Commun 2013, 49, 6674.

[33]. Li YL, Zhu L, Liu ZZ, Cheng R, Meng FH, Cui JH, Ji SJ, Zhong ZY, Angew. Chem. Int. Edit 2009, 48, 9914.

[34]. Engelgau MM, Narayan KMV, Herman WH, Diabetes Care 2000, 23, 1563. [PubMed: 11023153]

[35]. Hawkins SJ, Crompton LA, Sood A, Saunders M, Boyle NT, Buckley A, Minogue AM, McComish SF, Jiménez-Moreno N, Cordero-Llana O, Stathakos P, Gilmore CE, Kelly S, Lane JD, Case CP, Caldwell MA, Nat. Nanotechnol 2018, 13, 427. [PubMed: 29610530]

[36]. Villasenor R, Schilling M, Sundaresan J, Lutz Y, Collin L, Cell Rep. 2017, 21, 3256. [PubMed: 29241551]

[37]. Yan JP, Ilsley DD, Frohlick C, Steet R, Hall ET, Kuchta RD, Melancon P, J. Biol. Chem 1995, 270, 22836. [PubMed: 7559416]

[38]. McKinley BA, Morris WP, Parmley CL, Butler BD, Crit. Care Med 1996, 24, 1858. [PubMed: 8917037]

[39]. Nahrendorf M, Zhang HW, Hembrador S, Panizzi P, Sosnovik DE, Aikawa E, Libby P, Swirski FK, Weissleder R, Circulation 2008, 117, 379. [PubMed: 18158358]

[40]. Mora E, Smith EM, Donohoe C, Hertz DL, Am. J. Cancer. Res 2016, 6, 2416; [PubMed: 27904761] Cairncross JG, Wang MH, Jenkins RB, Shaw EG, Giannini C, Brachman DG, Buckner JC, Fink KL, Souhami L, Laperriere NJ, Huse JT, Mehta MP, Curran WJ, J. Clin. Oncol 2014, 32, 783; [PubMed: 24516018] De Witt M, Gamble A, Hanson D, Markowitz D, Powell C, Al Dimassi S, Atlas M, Boockvar J, Ruggieri R, Symons M, Mol. Med 2017, 23, 50; [PubMed: 28386621] Mora E, Smith EML, Donohoe C, Hertz DL, Am. J. Cancer Res 2016, 6, 2416. [PubMed: 27904761]

[41]. Pal S, Kozono D, Yang XD, Fendler W, Fitts W, Ni J, Alberta JA, Zhao J, Liu KX, Bian J, Truffaux N, Weiss WA, Resnick AC, Bandopadhayay P, Ligon KL, DuBois SG, Mueller S, Chowdhury D, Haas-Kogan DA, Cancer Res. 2018, 78, 4007; [PubMed: 29760046] Biery M, Myers C, Girard E, Morris S, Carmack S, Noll A, Sarthy J, Ferguson E, Mhyre A, Strand A, Olson J, Vitanza N, Neuro-Oncology 2018, 20, 56;Creasy CL, Nat. Med 2017, 23, 413. [PubMed: 28388610]

[42]. Olmez I, Brenneman B, Xiao A, Serbulea V, Benamar M, Zhang Y, Manigat L, Abbas T, Lee J, Nakano I, Clin. Cancer Res 2017, 23, 6958; [PubMed: 28814434] Bronner SM, Merrick KA, Murray J, Salphati L, Moffat JG, Pang J, Sneeringer CJ, Dompe N, Cyr P, Purkey H, Bioorg. Med. Chem. Lett 2019.

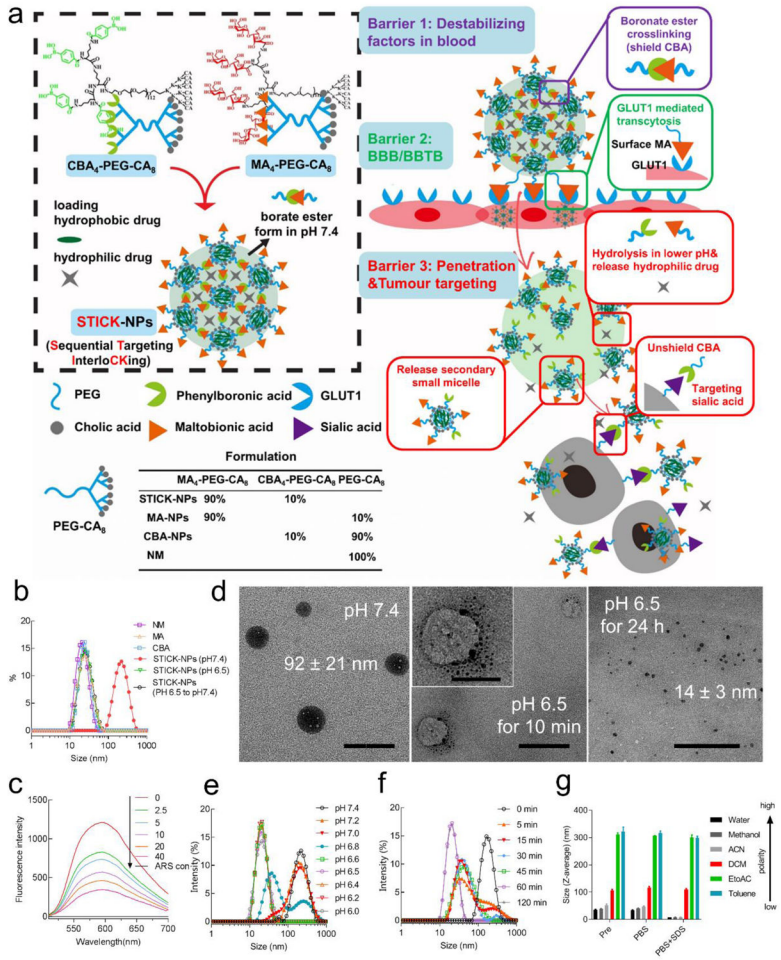

Figure 1.

a) Design of transformable STICK-NPs and detailed multi-barrier tackling mechanisms to brain tumors. The pair of targeting moieties selected to form **S**equential **T**argeting **I**n **C**rosslin**K**ing (STICK) were maltobionic acid (MA), a glucose derivative, and carboxyphenylboronic acid (CBA), one type of boronic acid, and were built into our well-characterized self-assembled micelle formulations (PEG-CA_8). STICK-NPs were assembled by a pair of MA_4-PEG-CA_8 and CBA_4-PEG-CA_8 with the molar ratio of 9:1 while inter-micelle boronate crosslinkages, STICK, formed between MA and CBA resulting in larger nanoparticle size. Excess MA moieties were on the surface of the nanoparticles, while CBA moieties were firstly shielded inside the STICK to avoid non-specific bindings. Hydrophobic drugs were loaded in the hydrophobic cores of secondary small micelles, while hydrophilic agents were trapped in the hydrophilic space between small micelles. In the following studies we included several control micelle formulations including NM (no targeting), MA-NPs (single BBB targeting), and CBA-NPs (single sialic acid tumor targeting) nanoparticles (inserted table). In detail, STICK-NPs could overcome **Barrier 1** (destabilizing condition in the blood) by intermicellar crosslinking strategy, **Barrier 2** (BBB/BBTB) by active GLUT1 mediated transcytosis through brain endothelial cells, and **Barrier 3** (penetration & tumor cell uptake) by transformation into secondary smaller micelles and reveal of secondary

active targeting moiety (CBA) against sialic acid overexpressed on tumor cells in response of acidic extracellular pH in solid tumors. b) Intensity-weighted distribution of MA-NPs, CBA-NPs, NM, and STICK-NPs at pH 7.4 and 6.5. c) Boronate ester bond formation verified by a fluorescence assay based on the indicator of alizarin red S (ARS) (Ex: 468 nm, 0.1 mg/mL). ARS fluorescence decreased along with a dose-dependent increase of MA_4-PEG-CA_8 concentrations from 0 μM to 40 μM (fixed CBA_4-PEG-CA_8 with 2.5 μM). This demonstrated the formation of boronate ester bonds between MA_4-PEG-CA_8 and CBA_4-PEG-CA_8. d) Transmission electron micrograph (TEM) imaging for visualizing the transformation process of STICK-NPs (92 ± 21nm) into secondary small micelles (14 ± 3nm) when changing from pH 7.4 to pH 6.5 at 10 mins (intermediate status) and 24 hours. Of note, the low-contrast nanoparticle outline in the intermediate status represented the empty large nanoparticle with associated secondary small micelles outside. Scale bar, 200 nm or 100 nm (insert). pH-dependent (e) and time-dependent (f) intensity-weighted distribution changes of STICK-NPs under pH 6.5. pH 6.8 appears to be the cut-off value for triggering micelle transformation. g) The Z-average size of STICK-NPs that was formulated with different solvents (various polarities) and treated with sodium dodecyl sulfate (SDS) or not in PBS. ACN: acetonitrile; DCM: dichloromethane; EtOAc: ethyl acetate.

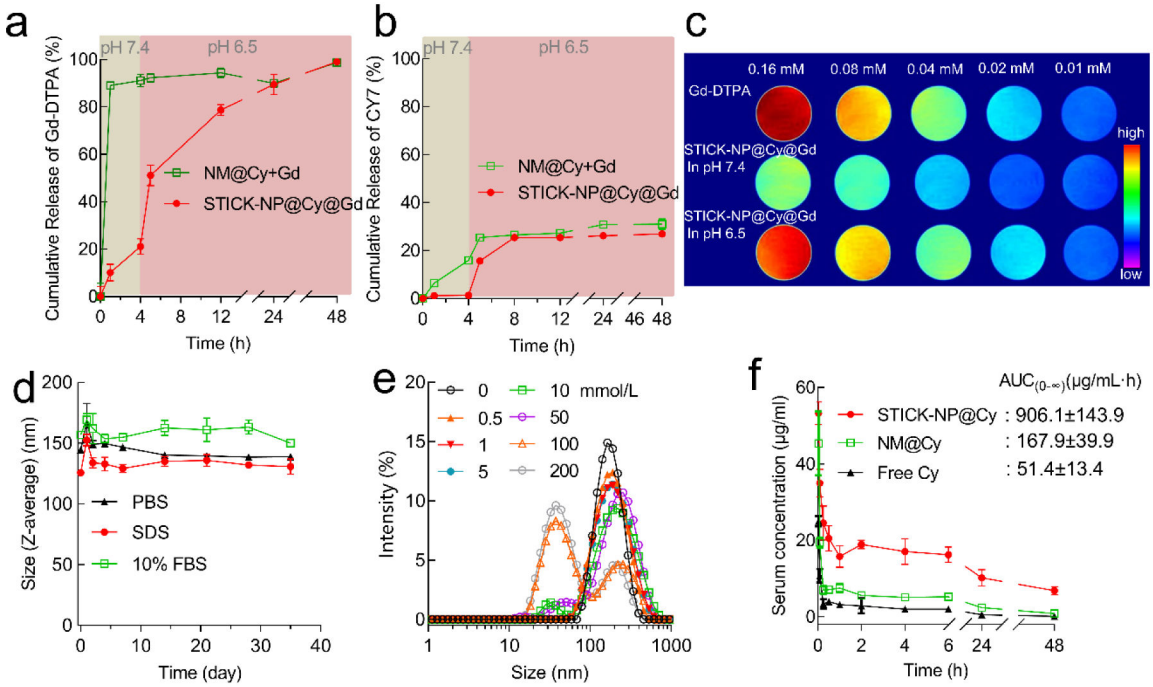

Figure 2.

Cumulative release profile for both hydrophilic (Gd-DTPA) (a) and hydrophobic (Cy7.5) payloads (b) from STICK-NPs and NM in the presence of different pH. A mixture of NM and free Gd was used in (a), as Gd could not be loaded into NM. Drug release study was performed initially at pH 7.4 PBS (grey areas) and was then subjected to pH 6.5 after 4 h (pink areas). Samples were collected at different time points and were measured by inductively coupled plasma mass spectrometry (ICP-MS) for Gd-DTPA level and fluorescence spectrometer for the concentration of Cy7.5. (n = 3). c) *In vitro* T_1-weighted MRI signal of Gd-DTPA, and STICK-NP@Cy@Gd under pH7.4 or pH6.5 at different concentrations acquired by a Bruker Biospec 7T MRI scanner. d) The Z-average size stability test of STICK-NP@Cy@Gd in the presence of PBS, 10 mg/mL SDS or 10% FBS. (n = 3) e) The intensity-weighted distribution changes of STICK-NPs in the presence of different concentrations of glucose (mmol/L). Of note, normal human serum glucose level ranges from 3.9 to 5.5 mmol/L. f) Pharmacokinetic profiles of free Cy7.5, STICK-NP@Cy, and NM@Cy (Cy7.5, 10 mg/kg) in jugular vein catheterized rats (n = 3). Serum was collected at different time points, and drug concentrations were measured based on fluorescence signals. The error bars were the standard deviation (SD).

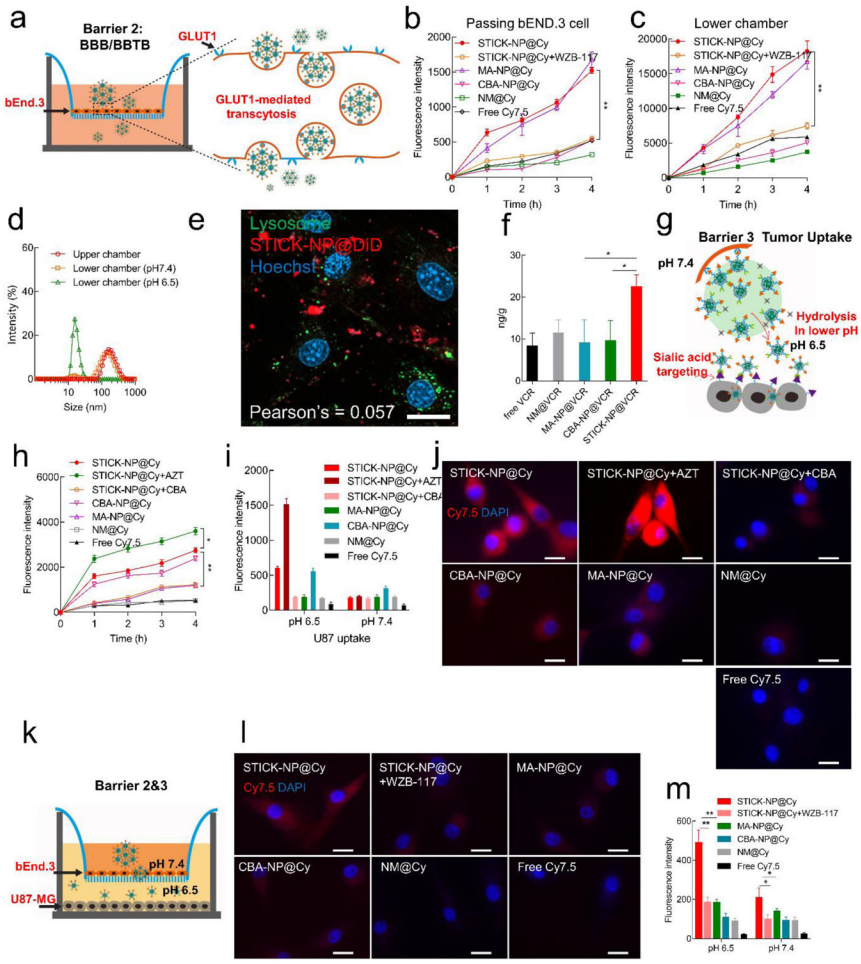

Figure 3.

Multi-barrier tackling mechanism studies for STICK-NPs mediated brain tumor drug delivery process *in vitro*. a) Diagram for Transwell® (0.4 μm pore size) modeling for Barrier 2 (BBB/BBTB), and the STICK-NP@Cy mediated transcytosis through brain endothelial cells. Mouse brain endothelial cells (bEnd.3) were cultured in the upper chamber. b) Quantitative measurements for the intracellular fluorescence intensity of Cy7.5 in bEnd.3 cells. bEnd.3 cells were incubated with free Cy7.5, STICK-NP@Cy, MA-NP@Cy, CBA-NP@Cy and NM@Cy (Cy7.5: 0.1 mg/mL) and lysed at different time points. To inhibit GLUT1 activity, cells were pre-treated with 40 μM WZB-117 for 1 hour before cellular uptake study in the following (b-c). (n = 3, **p<0.01, two-way ANOVA). c) The efficiency of the transcytosis of different formulations with Cy7.5 in the Transwell system as (a). Mouse bEnd.3 cells were seeded in the upper chamber to form a tight junction that was confirmed with > 200 Ω.cm^2 trans-endothelial electrical resistance (TEER). Free Cy7.5, MA-NP@Cy, CBA-NP@Cy, NM@Cy, and STICK-NP@Cy were loaded in the upper chamber and medium in the lower chambers were collected at different time points to measure the fluorescence intensity of Cy7.5. d) The intensity-weighted distribution of the STICK-NP@Cy presented in the upper chamber, and lower chamber with medium adjusted to pH 7.4 and 6.5, respectively. The size was measured by DLS. n = 3. e) Representative confocal image of the subcellular distribution of STICK-NP@DiD (red) in the bEnd.3 cells

after 1 hour of incubation. Lysotracker (green): lysosome; Hochst 33342 (blue) : nuclear staining; Scale bar = 20 μm. f) VCR concentrations in normal brain tissue in Balb/c mice with intact BBB at 6 hours post-intravenous injection of STICK-NPs@VCR and other formulations (2 mg/kg). The whole brains were homogenized. VCR was extracted and the concentrations were measured by liquid chromatography-mass spectrometry (LC-MS). g) The diagram depicting barrier 3 - tumor uptake and pH-dependent transformation with newly revealed CBA for sialic acid-mediated tumor targeting. h) Quantitative fluorescence measurement of total intracellular Cy7.5 with the same treatment at different time points. The Cy7.5 fluorescence intensity was measured through the lysed cells. n = 3, **$p<0.01$, two-way ANOVA. Scale bar = 20 μm. Representative quantitive analysis (i) and fluorescence images (j) of U87-MG cellular uptake of free Cy7.5, MA-NP@Cy, CBA-NP@Cy, NM@Cy and STICK-NP@Cy (Cy7.5: 0.1 mg/mL) under different pH (7.4 and 6.5) at 1 hour time point. In one parallel group treated STICK-NPs, the sialic acid expression on the tumor cell surface was augmented with 40 μM azidothymidine (AZT). In another parallel group of treated STICK-NPs, 40 μM free CBA were added to compete with the surface CBA (secondary targeting moiety) on the secondary STICK-NPs. n = 3, **$p<0.01$, two-way ANOVA. k) The diagram of Transwell (0.4 μm pore size) co-culture system with the bEND3 cells in the upper chamber and U87-MG cells in the lower chamber to model Barriers 2+3. Representative fluorescence images (l) and quantitive analysis (m) of U87-MG cells at 1 hour after treatment with free Cy7.5, MA-NP@Cy, CBA-NP@Cy, NM@Cy and STICK-NP@Cy (Cy7.5: 0.1 mg/mL) in the upper chamber. After adding in the upper chamber for one hour, the lower chamber medium was adjusted to pH 7.4 or 6.5 for another hour and the U87-MG cells at lower chamber were incubated for another hour. In a parallel group treated STICK-NPs, GLUT1 activity was pre-inhibited by WZB-117. Scale bar = 20 μm. The error bars were the standard deviation (SD).

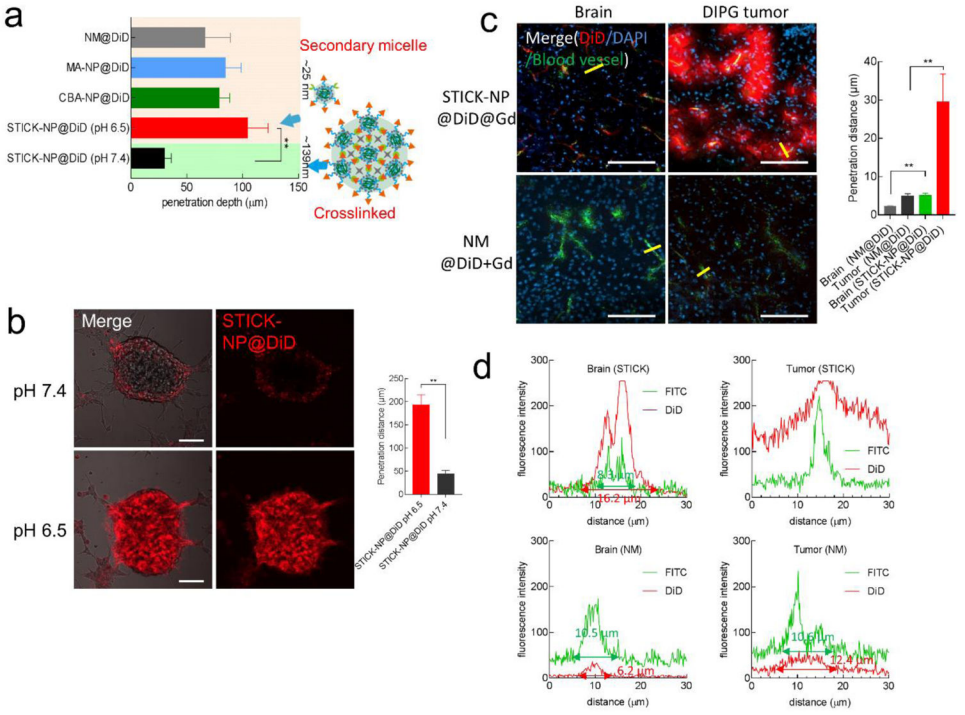

Figure 4.

Transforming-dependent tumor penetration study for STICK-NPs. a) Quantitative analysis of the penetration in U87-MG-GFP neurosphere with STICK-NP@DiD (pH 7.4 and 6.5) and other formulations (pH 7.4). The Z-average size of STICK-NP@DiD (pH 7.4) was 138.6 ± 11.8 nm, while STICK-NP@DiD (pH6.5) and other nanoformulations were around 25 nm (Figures S4,5, Supporting information). n = 3. *t*-test, **P < 0.01. b) The representative images and quantitative analysis of the penetration of STICK-NP@DiD (red) into DIPG tumor spheroid at 24 hours under pH 7.4 and 6.5. (DiD: 0.05 mg/mL). n = 3. *t*-test, **P < 0.01. Scale bar, 100 μm. c) Tissue penetration of STICK-NP@DiD at the normal brain area and implanted DIPG area from the orthotopic mouse model at 16 hours post-injection of STICK-NP@DiD and NM@DiD (Red, 5mg/kg). DIPG-XIII-P cells were injected into the mouse brainstem to establish the orthotopic model. DIPG bearing mice were injected with STICK-NP@DiD and NM@DiD (Red, 5mg/kg) for 16 hours. Before sacrificing the mice, Dextran-FITC (green, moleclular weight = 70 K) were injected to highlight blood vessels. Penetration distance from the blood vessels was analyzed with Image J (right). DAPI (blue): nuclear staining. Scale bar = 100 μm. d) Tissue penetration analysis of STICK@DiD and NM@DiD (Red) beyond the blood vessels (FITC, green) at both normal brain and DIPG tumor sites corresponding to the cross-sections (yellow line) in (c).

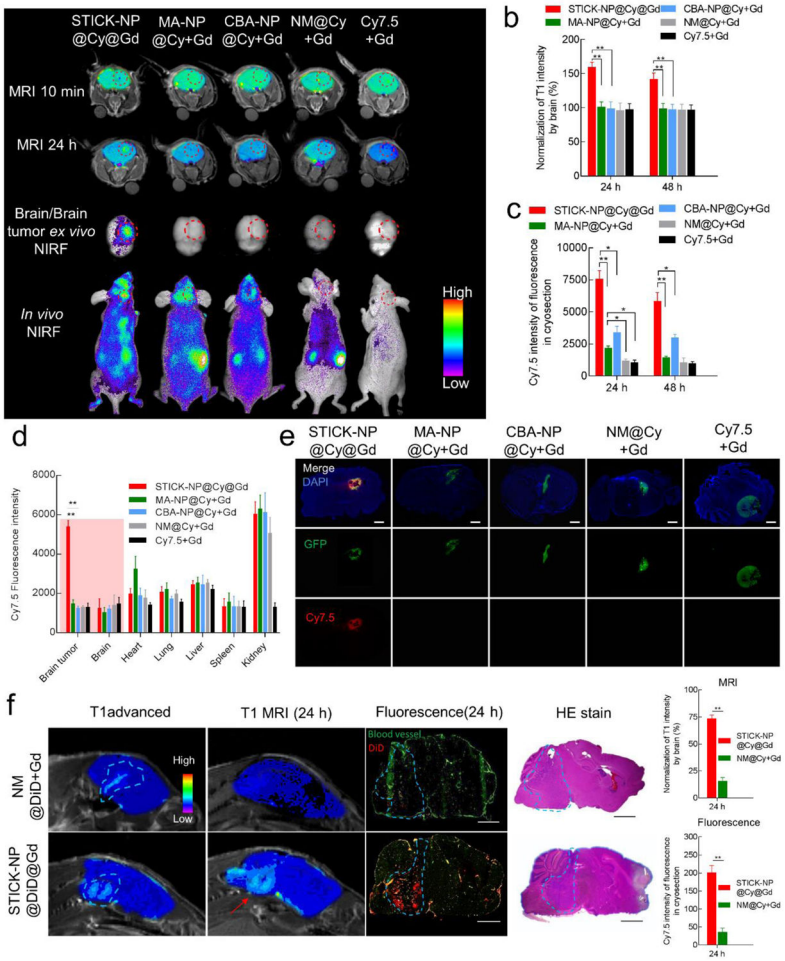

Figure 5.

Dual-modality imaging (MRI & NIRF imaging)-guided delivery process of STICK-NPs in orthotopic PDX GBM and PDX DIPG brain tumor models a) *In vivo* T_1-weighted MRI and NIRF images (*in vivo* and *ex vivo*) on PDX GBM bearing mouse model as indicated time points after iv injections of Cy7.5+Gd, MA-NP@Cy+Gd, CBA-NP@Cy+Gd, NM@Cy+Gd or STICK-NP@Cy@Gd (Gd-DTPA: 25 mg/kg; Cy7.5: 10 mg/kg). Since hydrophilic Gd-DTPA could not be loaded in MA-NP, CBA-NP, NM, free Gd-DTPA was given in conjunction with Cy7.5 loaded nanoparticles as controls. Tumor location was double-verified with T_2-weighted MR imaging. b) Quantitative analysis of MRI T_1 signal intensity normalized to normal brain tissue. *t*-test, **p<0.01. c) The NIRF intensity analysis of orthotopic brain tumors based on the whole mouse *in vivo* imaging at 24 and 48 hours post-injection. n = 3, *t*-test, **p<0.01, *p<0.05. d) Biodistribution analysis based on the Cy7.5 fluorescence intensity (*ex vivo* NIRF imaging) in PDX GBM bearing mice at 24 hours pos-injections of Cy7.5+Gd, MA-NP@Cy+Gd, CBA-NP@Cy+Gd, NM@Cy+Gd, and STICK-NP@Cy@Gd. n = 3, *t*-test, **p<0.01. e) Representative confocal images from the cryosection of the mouse brain with implanted GBM tumors at 24 hours post-injection of Cy7.5+Gd, MA-NP@Cy+Gd, CBA-NP@Cy+Gd, NM@Cy+Gd, and STICK-NP@Cy@Gd. Blue: DAPI; Green: U87-MG-GFP; Red: Cy7.5. Scale bar = 500 μm. The error bars were the standard deviation (SD). f) T_1-weighted MRI and confocal fluorescence imaging, with

quantitative analysis, on orthotopic PDX DIPG brain tumor model at 24 hours post-administration of NM@Cy+Gd or STICK-NP@DiD@Gd (Gd-DTPA: 25 mg/kg; DiD: 5 mg/kg as indicated. Before sacrificing the mice, animals were injected with Dextran-FITC(green) to highlight blood vessels. Red: DiD; Scale bar = 2 mm.

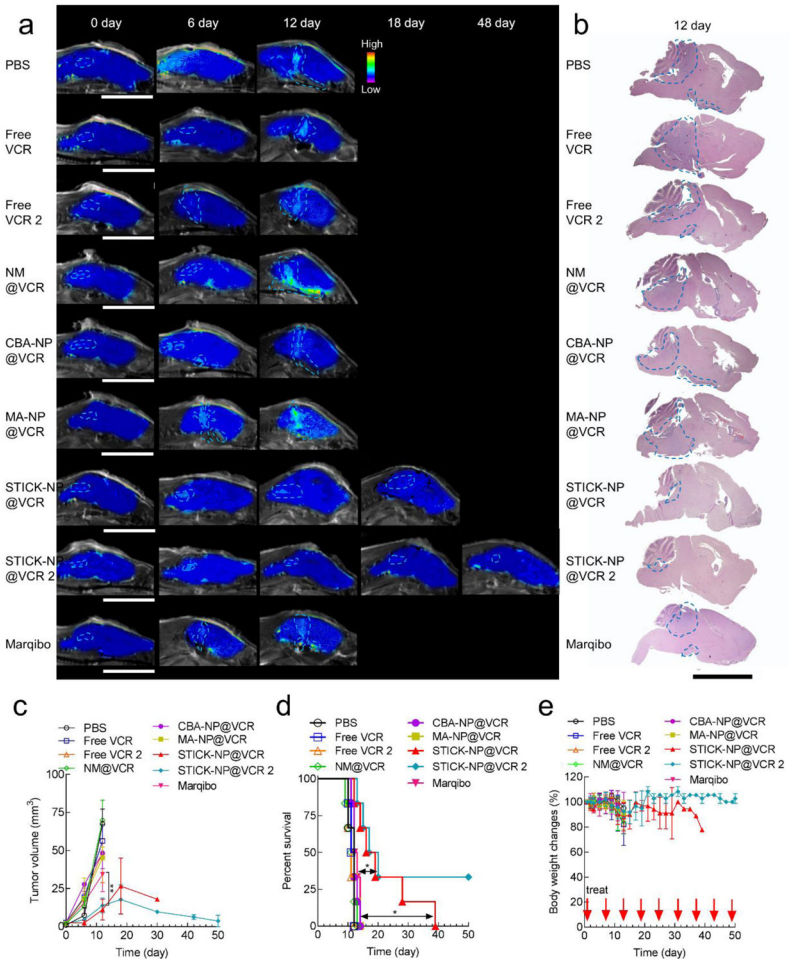

Figure 6.

Anti-cancer efficacy studies of STICK-NPs@VCR in the orthotopic PDX DIPG mouse model a) Tumor progression (blue dotted outline) of orthotopic DIPG mouse model monitored with Gd-enhanced T_1-weighted MRI of the same representative mouse from each group on day 0, 6, 12, 18 and 24 day after treatment with PBS, free VCR, NM@VCR, MA-NP@VCR, CBA-NP@VCR, STICK-NP@VCR, Marqibo® (VCR 1.5 mg/kg) free VCR2 and STICK-NM@VCR2 (VCR 2 mg/kg) every six days (intravenous injection). Scale bar =10 mm. b) Actual tumor burden was confirmed with histopathology (blue dotted outline) on day 12 post-injection from the same representative mouse with MRI results in (a). Scale bar = 5 mm. c) Quantitative analysis of the tumor growth curve based on MRI, Kaplan–Meier survival curve (d), and body weight changes (e) of the DIPG bearing mice after treatment of STICK-NP, Marqibo®, and other formulations. n = 6. *t*-test for tumor burden analysis; Log-rank (Mantel-Cox) test for survival time analysis. **p<0.01, *p < 0.05. Of note, all the mice in the treatment groups of PBS, free VCR, NM@VCR, MA-NP@VCR and CBA-NP@VCR died after day 12, while there were survivors in the STICK-NP@VCR groups. Therefore, the tumor growth curve and body weight changes were only plotted based on survived mice in STICK-NP@VCR groups beyond day 12.